







REPORT



Dilute-and-shoot analysis of therapeutic monoclonal antibody variants in fermentation broth: a method capability study

Christof Regl ^{*a,b}, Therese Wohlschlager ^{*a,b}, Wolfgang Esser-Skala ^{a,b}, Iris Wagner ^{a,b}, Martin Samonig^{a,b,c}, Johann Holzmann ^{b,d}, and Christian G. Huber ^{a,b}

^aDepartment of Biosciences, Bioanalytical Research Labs, University of Salzburg, Salzburg, Austria; ^bChristian Doppler Laboratory for Innovative Tools for Biosimilar Characterization, University of Salzburg, Salzburg, Austria; ^cThermo Fisher Scientific GmbH, Germering, Germany; ^dTechnical Development Biosimilars, Global Drug Development, Novartis, Sandoz GmbH, Kundl, Austria

ABSTRACT

Monoclonal antibodies (mAbs) are widely applied as highly specific and efficient therapeutic agents for various medical conditions, including cancer, inflammatory and autoimmune diseases. As protein production in cellular systems inherently generates a multitude of molecular variants, manufacturing of mAbs requires stringent control in order to ensure safety and efficacy of the drugs. Moreover, monitoring of mAb variants in the course of the fermentation process may allow instant tuning of process parameters to maintain optimal cell culture conditions. Here, we describe a fast and robust workflow for the characterization of mAb variants in fermentation broth. Sample preparation is minimal in that the fermentation broth is shortly centrifuged before dilution and HPLC-MS analysis in a short 15-min gradient run. In a single analysis, *N*-glycosylation and truncation variants of the expressed mAb are identified at the intact protein level. Simultaneously, absolute quantification of mAb content in fermentation broth is achieved. The whole workflow features excellent robustness as well as retention time and peak area stability. Additional enzymatic removal of *N*-glycans enables determination of mAb glycation levels, which are subsequently considered in relative *N*-glycoform quantification to correct for isobaric galactosylation. Several molecular attributes of the expressed therapeutic protein may thus be continuously monitored to ensure the desired product profile. Application of the described workflow in an industrial environment may therefore substantially enhance in-process control in mAb production, as well as targeted biosimilar development.

ARTICLE HISTORY

Received 11 October 2018
Revised 21 November 2018
Accepted 14 December 2018

KEYWORDS

Multiple attribute monitoring; MAM; monoclonal antibodies; high-performance liquid chromatography; electrospray ionization mass spectrometry; fermentation; antibody subunits; glycation; glycosylation; structural analysis; biosimilar; process analytical technology; PAT; process monitoring

Introduction

Industrial production of therapeutic monoclonal antibodies (mAbs) involves extensive clone selection and process optimization procedures, which are initially performed at small scale.^{1, 2} In this context, not only productivity and viability of the host cells are pivotal, but also the molecular composition and heterogeneity of the expressed mAb is of importance to ensure safety and efficacy of the drug. More specifically, quality attributes such as the glycosylation profile, truncation and incorrect assembly of mAb subunits, oxidation, deamidation and glycation are profoundly affected by the cell culture conditions, and therefore need proper control.^{3–12} Simultaneous monitoring of these attributes may thus enable instant tuning of process parameters, *e.g.*, temperature, pH value, and cultivation time, to achieve the desired product profile.^{1, 13}


In IgG1-type mAbs, *N*-glycosylation represents a critical quality attribute (CQA) because it affects the safety and efficacy of the therapeutic protein.¹⁴ This modification occurs at a conserved asparagine residue in the CH2 domain of the heavy chain and significantly affects protein structure and stability, antibody-dependent cell-mediated cytotoxicity (ADCC),

and complement-dependent cytotoxicity (CDC).^{8, 15, 16} An important example of *N*-glycan variability is the presence/absence of afucosylated glycans, which is known to affect the efficacy of therapeutic antibodies involving ADCC as a mechanism of action.^{17, 18} In contrast to *N*-glycosylation, the non-enzymatic addition of a hexose molecule to lysine residues is referred to as glycation, which may be induced during production and storage of a mAb.^{4, 5, 19} Normally, glycation represents a quality attribute of low criticality. However, if glycation occurs in the complementarity-determining region (CDR) of the mAb, its criticality may be high and therefore needs control.^{19–22}

For the purpose of process monitoring, mAb variants are typically purified from fermentation samples by protein A affinity chromatography before in-depth protein characterization is performed *via* a wide spectrum of analytical methods.²³ Typically, *N*-glycans are enzymatically released, fluorescently labelled and analyzed by high-performance liquid chromatography (HPLC) with fluorescence detection.^{23–25} In addition, proteolytic digestion and peptide mapping by HPLC hyphenated to mass spectrometry (MS) allows multiple attribute monitoring (MAM), for example, of

CONTACT Christian Huber  c.huber@sbg.ac.at  Department of Biosciences, Bioanalytical Research Labs, University of Salzburg, Hellbrunner Straße 34, Salzburg 5020, Austria

*These authors contributed equally to this work

 Supplemental data for this article can be accessed on the [publisher's website](#).

© 2018 The Author(s). Published with license by Taylor & Francis Group, LLC.

This is an Open Access article distributed under the terms of the Creative Commons Attribution-NonCommercial-NoDerivatives License (<http://creativecommons.org/licenses/by-nc-nd/4.0/>), which permits non-commercial re-use, distribution, and reproduction in any medium, provided the original work is properly cited, and is not altered, transformed, or built upon in any way.

glycosylation, glycation, deamidation, and oxidation.^{23,26,27} Despite the depth of information obtained, the suitability of these approaches for simultaneous monitoring of fermentation processes is limited due to lengthy sample preparation procedures and artefacts introduced during sample preparation.

In contrast, sample preparation for intact mAb analysis is minimal and may facilitate real-time monitoring of biotechnological processes.^{9,28,29} Intact protein mass determination allows confirmation of the elemental composition, profiling of glycosylation patterns, and detection of truncation variants.^{30–34} Furthermore, induction of artificial modifications during sample handling, *e.g.*, deamidation or oxidation, is minimized.^{35–37} Different approaches have been described for relative quantification of the intact mAb and mAb fragments purified from fermentation broth samples by protein A chromatography. Employing reversed-phase (RP) HPLC-MS, relative quantification of fully assembled, intact mAb, free light chain, light chain fragments, light chain dimer, and multiple forms of Fab' was accomplished.³⁸ Applying a similar analytical approach, mAb glycosylation variants were relatively quantified in simulated fermentation broth samples obtained by spiking a mAb drug product into serum-free cell culture medium.³⁹

Here, we provide a critical evaluation of the capabilities and limitations of HPLC-MS-based methodology for the direct analysis of the target protein and product-related variants in fermentation broth at the intact protein level. Employing an organic monolith-based ion-pair (IP)-RP-HPLC separation system and a hybrid quadrupole-Orbitrap MS platform, we relatively quantify *N*-glycosylation variants, while taking into account glycation levels. Furthermore, we relatively quantify product-related variants such as truncation variants and incorrectly assembled mAb subunits. Simultaneously, the target protein may be absolutely quantified based on online UV-detection. Finally, robustness and repeatability of the method are assessed with respect to retention time, peak area, and mass accuracy. Applicability of the analytical approach is demonstrated for samples drawn from a fermentation process and for the corresponding reference drug product. The described workflow may be implemented for the in-process control of mAb production processes, and, moreover, the approach represents a powerful tool to guide clone selection and process development during the targeted development of a biosimilar drug.

Results

Separation and identification of mAb variants and product-related variants

In order to assess the presence of mAb variants and product-related variants in fermentation samples drawn from a clone selection process, we implemented a fast analytical workflow involving minimal sample preparation, *i.e.*, only centrifugation and dilution. Fermentation broth is a relatively complex sample matrix that not only contains the fully-assembled mAb, but also intermediates and degradation products, host cell proteins, metabolites, and cell media components; hence, chromatographic separation prior to mass spectrometric

detection is essential. For this purpose, we performed IP-RP-HPLC employing a monolithic polystyrene-divinylbenzene (PS-DVB)-based column (50 × 1.0 mm i.d.) coupled *via* electrospray ionization (ESI) to a quadrupole-Orbitrap mass spectrometer (Thermo Scientific™ Q Exactive™). In addition, online detection by UV-spectroscopy at 214 nm was implemented. mAb species were then identified based on zero-charge mass spectra obtained by the Sliding Window Algorithm embedded in the Thermo Scientific™ BioPharma Finder™ 3.0 software. The analyzed samples were drawn from a mAb fermentation process at AMBR™ (advanced microscale bioreactor) scale (2.5 mL) after five days (day 5), ten days (day 10), and fourteen days (day 14) of fermentation. In addition, a sample of purified mAb obtained upon protein A affinity chromatography after 15 days of fermentation (capture eluate) was analyzed. Furthermore, the corresponding reference drug of the biosimilar candidate was analyzed. In order to compare the different samples varying in their mAb concentration, samples were diluted to obtain equivalent peak areas of the intact mAb. Ribonuclease A (RibA) was spiked as carrier protein to avoid adsorptive losses of low abundant protein species.⁴⁰

Chromatograms obtained by HPLC-UV-MS analysis of the above described samples are shown in Figure 1. Based on the most abundant molecular mass obtained for each chromatographic peak, several mAb variants and truncation products could be assigned, taking into account the theoretical molecular mass (Figure S-1). The most abundant chromatographic peak in all samples arises from the fully assembled mAb (peak 5, 149196.91 Da, −1.93 ppm mass deviation) corresponding to the most abundant glycosylation variant (A2G0F/A2G0F). A variant eluting slightly earlier (peak 4) was assigned to a glycosylated heavy chain dimer (HC₂, 101372.54 Da, −14.26 ppm). Peak 3 corresponds to a light chain dimer (LC₂, 46890.55 Da, −22.53 ppm) while peak 2 arises from a light chain monomer (LC, 23565.23 Da, −23.00 ppm). Peak 1 can be attributed to a glycosylated mAb truncation product (HC fragment, 23980.80 Da, +8.34 ppm). In addition to the above described major mAb species, the following minor variants were detected: cysteinylated LC, glycated LC-dimer, and different glycosylation variants of HC₂ and the intact mAb (Supplementary material, spreadsheet E-1). The carrier protein RibA eluted with the column hold-up volume and did not affect separation of mAb variants (Figure S-2).

Repeatability and mass accuracy of the applied HPLC-MS workflow were assessed by repetitive measurements in order to determine the confidence of mass determination and its implication in peak assignment. For this purpose, six technical replicates of fermentation sample day 14 were analyzed. The precision of molecular mass determination expressed as 95% confidence interval ranged from ±0.16 to ±2.89 Da (Table 1), implying that compounds differing by more than ±3 Da may be readily discerned by MS if separated prior to MS.

Column robustness and regeneration were maintained over more than 2000 injections. Since the column material utilized in our study was a PS-DVB-based monolith, which is chemically very stable, we did not detect a significant deterioration of column performance after 2000 injections. This is demonstrated in the supporting material by injection of a 50 ng mL^{−1}

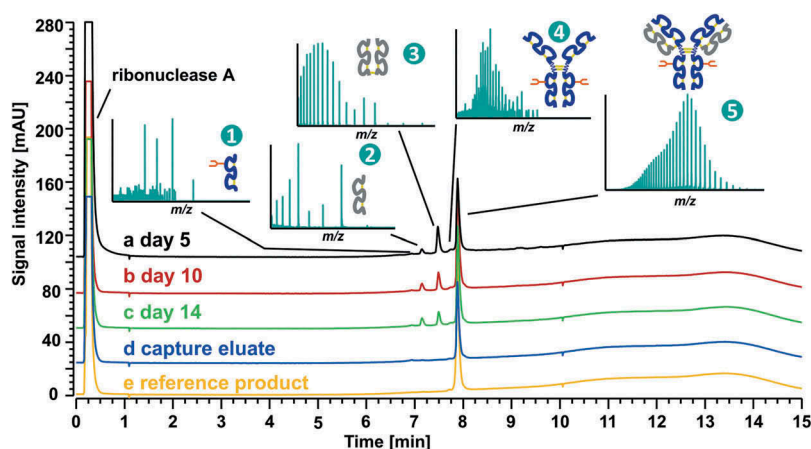


Figure 1. UV-traces of IP-RP-HPLC separations for mAb fermentation samples (a–c), protein A purified mAb (d), and reference drug product (e). Exemplary raw mass spectra used for peak assignment are indicated (1–5). The following mAb species were identified based on the most abundant mass, respectively: peak 1, HC truncation variant; peak 2, LC; peak 3, LC₂; peak 4, HC₂; peak 5, intact mAb. Details on peak identification are provided in Table 1. Mass spectra and deconvoluted masses of peaks 1–5 are displayed in Figure S-1 and in the Supplementary material, spreadsheet E-1. Sample load was normalized to the intensity of peak 5 obtained by injection of reference product at [10.0 ng μ L⁻¹]. The following dilutions were injected; 1:10 (day 5), 1:50 (day 10), 1:200 (day 14), 1:400 (capture eluate).

Table 1. Identified mAb species and accuracy of mass determination.

Peak ^a	Retention time [min] ^b	Identified mAb species ^c	Theoretical molecular mass [Da]	Average molecular mass [Da] ^b	Average mass deviation [Da] ^b	95% confidence interval [Da] ^b	Fractional abundance [%] ^b
1	7.05	HC fragment + A2G0F	23980.60	23981.83	0.53	0.52	0.08
2	7.26	LC + Cys	23567.79	23567.43	0.21	0.44	3.23
2	7.26	LC + 2 disulfides + Cys	23563.76	23563.54	0.15	0.35	2.34
3	7.61	LC ₂	46891.61	46890.43	0.48	0.16	18.95
3	7.61	LC ₂ + glycation	47053.75	47052.66	0.46	0.37	0.77
4	7.83	HC ₂ + A2G1F/GnF	101373.99	101374.56	0.57	1.47	0.18
5	8.00	Intact mAb + A2G0F/ A2G0F	149197.20	149195.72	0.61	0.23	48.78
5	8.00	Intact mAb + A2G0F/ A2G1F	149359.34	149359.55	0.12	0.24	15.49
5	8.00	Intact mAb + A2G0F/ A2G2F	149521.48	149522.55	0.49	0.63	4.54
5	8.05	Intact mAb + A2G1F/ A2G2F	149683.62	149684.44	1.07	2.89	0.79
5	8.05	Intact mAb + A2G0F/ A2G0	149051.06	149049.04	1.10	1.80	0.34

^aNumbers correspond to chromatographic peaks in Figure 1.

^bAverage derived from six measurements of sample day 14, all performed within three days.

^cGlycan annotation refers to Table S-1. Peak areas, retention times, deconvolution parameters, deconvoluted masses, deviations and corresponding calculations are provided in the Supplementary material, spreadsheet E-2.

solution of mAb reference material before and after 965 injections of mAb reference material or fermentation samples, in which the retention times and peak widths at half height differed by only 4.8 s and 0.06 s, respectively (Figure S-3). PS-DVB monolith-based column materials were also shown to exhibit significantly lower carryover compared to silica-based stationary phases.⁴¹ In order to investigate memory or carryover effects, we performed blank injections immediately after the injection of mAb reference material of different concentration. Figure S-4A shows the first and tenth blank run after loading of 10 μ L of a 250 ng \cdot mL⁻¹ injection of mAb solution. Due to the relatively high amount injected, 0.77% carryover was observed in the first blank analysis, whereas the peak area decreased to less than 0.032% after 10 blank runs. In the analysis of low concentrated mAb solutions (10 ng \cdot mL⁻¹), carryover became undetectable already after three blank runs. In consequence, mAb samples were always injected in increasing concentrations and analyses of calibration

standards and samples were generally separated by at least three blank runs.

Relative quantification of mAb variants and product-related variants

In the next step, we attempted relative quantification of the identified mAb species based on peak areas obtained from UV-spectroscopic detection (Table 2, top). The fractional abundance of peak 5 corresponding to the different glycosylation variants of the fully assembled mAb increased between day 5 of fermentation (72.2%) and day 10 (82.0%), while no significant change was observed between day 10 and 14. The relative increase of fully assembled mAb in the capture eluate (> 98%) demonstrates the efficiency of protein A purification. Moreover, the fractional abundance is similar to that of the reference product. The LC dimer (LC₂, peak 3) displays the highest fractional abundance of the identified

Table 2. Relative quantification of mAb species by HPLC-UV-MS.

Relative quantification of mAb species by UV-spectroscopy ^a									
Peak No.	RT [min] ^b	mAb species ^c	Molecular mass [Da] ^b	Day 5 ^d	Day 10 ^d	Day 14 ^d	Capture eluate ^d	Reference product ^d	
1	7.0	HC fragment	23980.95 (+14.5)	0.5 ± 0.6	0.5 ± 0.4	1.5 ± 0.5	1.3 ± 0.5	0.2 ± 0.1	
2	7.2	LC	23567.69 (-4.3)	3.4 ± 0.2	5.0 ± 0.3	6.2 ± 0.6	0 ± 0	0 ± 0	
3	7.5	LC ₂	46890.42 (-25.2)	19.4 ± 1.0	11.2 ± 0.5	9.4 ± 0.5	0 ± 0	0 ± 0	
4	7.8	HC ₂	101373.96 (-0.2)	4.4 ± 1.8	1.4 ± 0.1	1.1 ± 0.2	0.9 ± 0.2	1.0 ± 0.2	
5	7.9	Intact mAb	149196.92 (+1.9)	72.2 ± 2.0	82.0 ± 0.8	81.7 ± 1.4	97.8 ± 0.6	98.8 ± 0.1	
Relative quantification of mAb species by mass spectrometry ^a									
Peak No.	RT [min] ^b	mAb species ^c	Molecular mass [Da] ^b	Day 5 ^d	Day 10 ^d	Day 14 ^d	Capture eluate ^d	Reference product ^d	Average relative deviation UV vs. MS [%] ^f
1	7.1	HC fragment	23980.95 (+14.5)	0.2 ± 0.1	0.2 ± 0.3	0.3 ± 0.2	1.1 ± 0.6	0.1 ± 0.1	53.6
2	7.3	LC	23567.69 (-4.3)	1.2 ± 0.3	3.5 ± 0.9	4.3 ± 0.7	0 ± 0	0 ± 0	42.1
3	7.6	LC ₂	46890.42 (-25.2)	18.7 ± 2.0	14.3 ± 2.3	11.9 ± 1.4	0 ± 0	0 ± 0	2.1
4&5 ^e	8.0	HC ₂	101373.96 (-0.2)	79.9 ± 2.1	82.0 ± 3.5	83.5 ± 1.0	98.9 ± 0.6	99.9 ± 0.1	1.1
		Intact mAb	149196.92 (+1.9)						

^aRelative quantification based on chromatographic peak areas obtained for three technical replicates. Peak labels correspond to Figure 1. Peak areas, retention times, deconvolution parameters, deconvoluted masses, deviations and corresponding calculations are provided in the Supplementary material, spreadsheets E-1, E-3 & E-4.

^bRetention time and average mass determined for sample day 14 (average mass deviation in ppm).

^cQuantification includes modified mAb species, e.g. glycosylated and glycosylated variants

^dAverage relative abundance ± 95% confidence interval

^ePeak 4 and 5 co-elute in the total ion current chromatogram (TICC).

^fCalculated as the average of relative deviations of fractional abundances observed from UV-spectroscopy and TICC.

A supplementary Excel file containing data utilized for quantification and validation has been deposited at figshare.com and can be accessed via: <https://figshare.com/s/7991ee6d53fc86fcd016>

product-related variants in the fermentation samples, ranging from 19.4% (day 5) to 9.4% (day 14). This mAb species is neither detected in the capture eluate nor in the reference product. Also, the fractional abundance of the HC dimer (HC₂) decreases from 4.4% (day 5) to 1.1% (day 14) in the course of fermentation. Minimal amounts of HC₂ were detectable in the capture eluate (0.9%) and the reference product (1.0%). Monomeric LC (peak 2) increased from 3.4% (day 5) to 6.2% (day 14), but was not detected in the capture eluate and the reference product. Finally, the HC truncation product eluting in peak 1 was observed in the fermentation samples at fractional abundances up to 1.5%, in the capture eluate (1.3%), and in the reference product (0.2%).

In addition to UV-spectroscopic detection, we assessed relative quantification based on peak areas in total ion current chromatograms (TICC) as summarized in Table 2 (bottom). Co-elution of HC dimer and fully-assembled mAb (peak 4/5 in Figure S-5) can be attributed to the additional void volume arising from the connection between UV-cell and mass spectrometer. Fractional abundances obtained from the peak containing both HC₂ and intact mAb largely agree with fractional abundances determined by UV-detection (sum of peak 4 and 5), as expressed by an average relative deviation of 1.0%. Also, the fractional abundances of the major impurity, LC₂, were congruent (2.1% relative difference). For less abundant mAb species, differences in fractional abundances compared to UV detection were more pronounced as demonstrated by deviations of 42.1% (LC monomer) and 53% (HC fragment). Taking into account the superior chromatographic resolution, the robustness, and the absence of ion suppression effects, UV-detection is favorable for relative quantification compared to TICCs, especially when quantifying low abundant compounds.

Determination of glycation levels

Glycation results from the non-enzymatic attachment of a hexose to the ϵ -amino group of lysine residues. Since *N*-glycans in mAbs typically contain variable numbers of hexoses, *i.e.*, galactoses and mannoses, the presence of an additional hexose residue arising from glycation is indistinguishable upon intact mass determination. Unambiguous quantification of mAb *N*-glycosylation variants at the intact protein level thus requires consideration of glycation levels. In order to determine the extent of glycation, we enzymatically removed *N*-glycans using PNGase F. As glycation is not affected by the enzyme, glycation levels may subsequently be determined by HPLC-MS analysis. Interestingly, deglycosylation resulted in a slight, but significant retention time shift (+2.1 s, from 7.874 to 7.909 min, significance based on one-sided t-test: $p = 1 \cdot 10^{-10}$). At the same time, the peak width at half height decreased from 0.0598 ± 0.0004 to 0.0578 ± 0.0004 min (averages of six replicates $\pm 95\%$ confidence interval), corroborating the reduced heterogeneity of the deglycosylated mAb (for detailed data, see Supplementary material, spreadsheet E-5).

Comparison of deconvoluted spectra obtained for glycosylated (Figure 2(a)) and deglycosylated (Figure 2(b)) mAb in the reference product clearly reveals the expected shift to

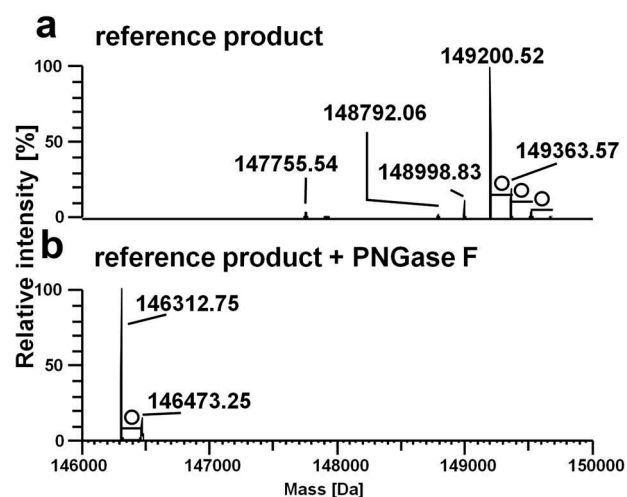


Figure 2. Determination of glycation levels by IP-RP-HPLC-MS. Deconvoluted mass spectra of intact mAb in reference product before (a) and after (b) PNGase F digest. Circles indicate additional hexose residues (+162 Da), originating from galactosylation or glycation. Details on data evaluation are provided in the Supplementary material, spreadsheet E-5.

lower *m/z* values upon removal of *N*-glycans. As no signals corresponding to the glycosylated mAb were observed in spectra of the deglycosylated samples (Figure 2(b)), the PNGase F digest can be considered complete. In addition to the deglycosylated mAb (Figure 2(b), 146312.75 Da), a glycosylated variant comprising an additional hexose residue, was present in the reference product as indicated by a mass shift of +162 Da. Employing this strategy, up to three glycosylations were detected in the deconvoluted spectra of the analyzed mAb fermentation samples, whereas one glycosylation was observed in the capture eluate (Figure S-6). Peptide mapping of the samples revealed partial glycation of 17 different lysine residues in total. Hotspots for glycation were identified both in the LC and the HC, (*e.g.*, LC: K183; HC: K139), displaying glycation levels of up to 2.2% (Table S-2).

For the purpose of relative quantification, extracted ion current chromatograms (XICCs) for 16 charge states of the different glycation variants were generated (Figure S-7). The mass range of XICCs used for relative quantification was calculated based on the full width at half maximum (FWHM) of each charge state. Average relative glycation levels of fermentation samples, capture eluate, and reference product were calculated based on the peak areas of technical triplicates and are shown in Figure S-8. The analyzed fermentation samples contained singly-glycosylated species up to 23.2% (day 10), while four-fold-glycosylated species were observed up to 2.1% (day 14). Interestingly, glycation levels did not increase during fermentation. The capture eluate contained 4.9% of singly glycosylated mAb, while the reference product contained 12.6% of this variant. Relative standard deviations ranged from 9.3% for the singly-glycosylated variant (15–20% fractional abundance) to 17% for the fourfold-glycosylated variant (1.4–2.1% fractional abundance). Notably, mAb variants modified with up to four glycosylations were only detectable by XICCs, *i.e.*, at the raw data level, but were not present in deconvoluted spectra, signifying elimination of low abundant signals during the deconvolution process.

Assignment of mAb glycosylation variants

In the next step, we aimed at assigning specific *N*-glycosylation variants to the masses determined for intact mAb species eluting with chromatographic peak 5 (Figure 1). For this purpose, sliding window deconvolution of summed mass spectra was performed for peak 5. Using the built-in Chinese hamster ovary (CHO) cell *N*-glycan library of the BioPharma Finder™ software, specific *N*-glycoforms could be assigned to the obtained masses for fermentation samples, capture eluate and reference product (Figure 3). Application of the *N*-glycan library restricts the number of possible structures based on prior knowledge about the glycan repertoire of CHO cells. Assignment of glycan structures is therefore based on previous knowledge and not on *de novo* structural characterization.

In total, 11 different glycoforms substituted with one or two *N*-glycans were identified. The fermentation sample drawn after five days displayed the most complex glycosylation pattern comprising at least eight different glycoforms, with the A2G0F/A2G1F form being the most abundant variant (Figure 3(a), for structures see Table S-1). In the course of fermentation, complexity of the glycoform pattern reduced to six major variants comprising shorter *N*-glycan structures, with the A2G0F/A2G0F glycoform being the most prominent,

as evidenced by mass spectra obtained for samples drawn at day 10 and day 14 (Figure 3(b,c)). The distribution of glycoforms was largely unaffected by protein A affinity chromatography, as demonstrated for the capture eluate (Figure 3(d)). Indeed, the glycosylation pattern of the latter highly resembled the glycoform distribution observed for the reference product (Figure 3(e)), thus representing a basis for glycosylation pattern comparability studies. A minor variant attributed to A1G0F/A1G0F was only present in the reference product.

Glycan structures assigned for the intact mAb were corroborated by peptide analysis upon tryptic digestion. In total, 12 *N*-glycan structures were identified in the mAb fermentation harvest samples, capture eluate and reference product (Table S-3). In addition, the non-glycosylated variant of the corresponding peptide (EEQYNSTYR) was detected. In accordance with the *N*-glycoforms detected at the intact mAb level, the most abundant structures comprised complex-type *N*-glycans substituted with up to two galactose residues, *i.e.*, A1G0F, A2G0F, A2G1F, A2G2F, and afucosylated A2G0. In addition to the *N*-glycan structures annotated for the intact mAb, six minor variants were identified at the glycopeptide level, all of which comprised fractional abundances below 0.5% (Table S-3). In turn, one glycan structure assigned at

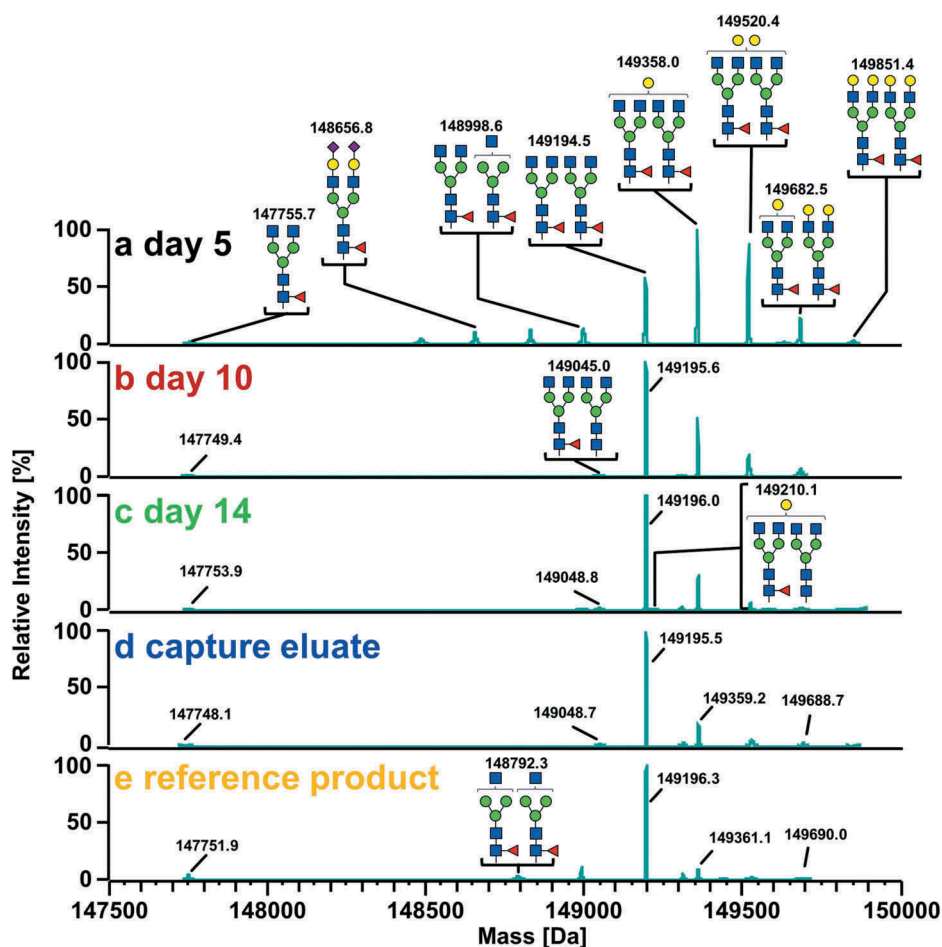


Figure 3. Deconvoluted mass spectra of intact mAb glycosylation variants in fermentation samples (a–c), capture eluate (d), and reference product (e). Each peak is annotated with the most probable combination of glycan structures. Glycoform annotations were derived from a CHO cell *N*-glycan library implemented in the BioPharma Finder™ software. A detailed mass list including deviations and deconvolution settings is provided in the Supplementary material, spreadsheet E-9.

the intact mAb level was not detected in the glycopeptide analysis (A2G2FSA2). This may be explained by lower ionization efficiency or stability of the *N*-glycopeptide substituted with two sialic acids compared to the intact glycoform. High-mannose type *N*-glycans were neither detected for the intact mAb nor on the glycopeptide level.

Relative quantification of mAb glycoforms

In order to deduce fractional abundances of the different glycoforms from raw spectra of the intact mAb, we generated XICCs based on the theoretical masses of the respective species (Figure S-7). The average fractional abundance of each *N*-glycoform was derived from peak areas in XICCs of triplicate measurements of fermentation samples, capture eluate, and reference product (Supplementary material, spreadsheet E-11). Importantly, additional hexose residues arising from glycation will not be discerned in this quantification strategy and thus introduce a bias in the obtained fractional abundances. In order to derive unbiased glycoform levels, we therefore corrected the fractional abundances considering previously determined levels of glycation (Figure S-8).

The correction mostly affected fractional abundances of glycoforms A2G0F/A2G0F and A2G0F/A2G1F, in that the

former increased while the latter decreased. For example, the A2G0F/A2G0F variant shifted from 49.6% (observed) to 77.7% (corrected) fractional abundance for sample day 10. On the other hand, correction of the fractional abundance of the A2G0F/A2G1F glycoform resulted in a decrease from 24.7% (observed) to 10.5% (corrected) in the same sample (Figure S-9).

Corrected fractional abundances of the three main glycoforms detected in the fermentation sample drawn at day 5 were as follows (Figure 4(a)): A2G0F/A2G1F (35.8%); A2G0F/A2G2F or A2G1F/A2G1F (27.0%); A2G0F/A2G0F (23.4%). In the course of fermentation, the fractional abundance of the A2G0F/A2G0F variant increased to 78.2% (day 14), while the abundance of the other glycoforms decreased below 10% (Figure 4(a)). The fractional abundances of the A2G0F/A2G0F variant were similar in the capture eluate and the reference product, amounting to 70.4% and 76.7%, respectively. The glycoform A2G0F/A1G0F was determined at a fractional abundance of 8.2% in the reference product, while fractional abundances in fermentation broth samples and capture eluate were below 1%. The glycosylation patterns depicted in Figure 3 clearly reveal that most of the glycans (>98–99%) carried a core fucose. The glycoform comprising a non-fucosylated glycan A2G0/A2G0F was detected at levels

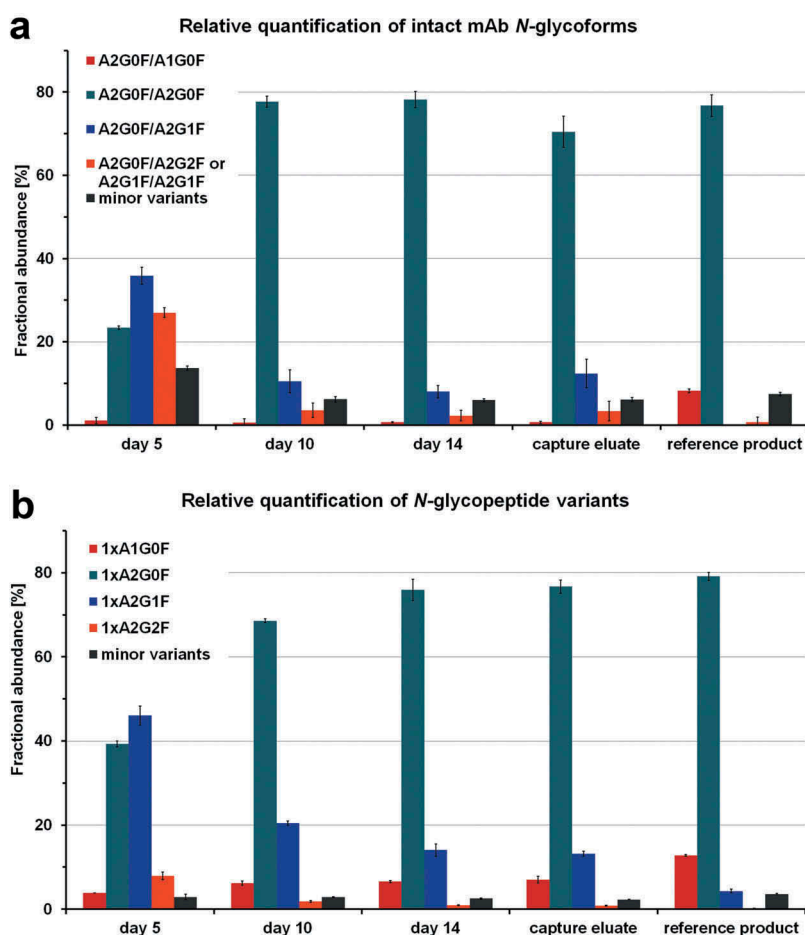


Figure 4. Relative quantification of mAb *N*-glycoforms. Fractional abundances (sum of all glycoform abundances corresponds to 100%) were determined at the intact mAb level based on XICCs (a) and at the glycopeptide level (b). Abundances displayed in (a) were corrected for glycation levels as described. Fractional abundances are based on three technical replicates; error bars indicate the 95% confidence interval. Details on data evaluation are provided in the Supplementary material, spread-sheet E-10 and E-11.

of up to 1.52% ($\pm 0.55\%$, 95% confidence interval (C.I.)) in fermentation samples and capture eluate, while it amounted to only 0.11% ($\pm 0.18\%$, 95% C.I.) in the reference product.

In addition to relative quantification of intact mAb glycoforms, we assessed fractional abundances derived from glycopeptide analysis (Figure 4(b), Table-S3): in fermentation sample day 5, the A2G1F *N*-glycopeptide predominated at 46.0% abundance, followed by A2G0F (39.3%), A2G2F (7.9%) and A1G0F (3.9%). The preponderance of A2G1F and A2G0F *N*-glycopeptides is in accordance with the intact mAb data, in that the *N*-glycoform substituted with these two structures is the most abundant in sample day 5 (Figure 4(a)). In the course of fermentation, the fractional abundance of A2G0F increased to 76.0% (day 14) while that of A2G1F decreased to 14.1%. A similar glycan distribution was observed in the capture eluate with abundances of 76.7% (A2G0F) and 13.2% (A2G1F). The abundance of the A2G0F glycopeptide in the capture eluate was similar to that obtained for the reference product (79.1%). Differences between capture eluate and reference product were observed with regard to A2G1F (13.2% vs. 4.3%) and A1G0F (7.0% vs. 12.8%). Sialylated variants were below 0.1% relative abundance in the capture eluate and were not detected in the reference product.

As mass spectrometric signal intensities are inherently affected by the ionization efficiency of the respective analytes, different ionization properties of intact mAb variants and glycopeptides may affect the derived fractional abundances. For a small analyte such as a peptide, the impact of the glycan on ionization efficiency is expected to be more pronounced compared to the intact protein. We therefore further evaluated trueness and precision of intact mAb glycoform quantification.

Trueness and precision of mAb glycoform quantification

The absence of validated mAb standards impedes direct evaluation of the trueness of glycoform quantification by mass spectrometry. In order to assess concentration dependence of mass spectrometric signal intensities for the observed glycosylation variants of the intact mAb, we analyzed mixtures of samples comprising different concentrations of the respective glycoforms. Comparison of the obtained concentration-

response curves with the expected peak ratios (conventional true value) then allowed determination of the trueness of relative quantification.

For this purpose, the samples differing most in their glycosylation patterns were assessed. Accordingly, fermentation sample day 5 and reference product were mixed at ratios of 10:0, 9:1, 7:3, 5:5, 3:7, 1:9, and 0:10 (*v/v*) at final concentrations of $10 \text{ ng}\mu\text{L}^{-1}$ of the mAb and analyzed in quintuplicates. Fractional abundances obtained for sample day 5 (10:0) and for the reference product (0:10) were considered true values for 0% and 100% and used for the calculation of the other conventional true values. The respective fractional abundances and conventional true values of two exemplary glycosylation variants were plotted against the amount of reference product in percent (Figure 5, Supplementary material, spreadsheets E-12 and E-13). As expected, the fractional abundance of the A2G0F/A2G0F glycoform increases with the amount of reference product present in the mixture (Figure 5(a)). For all mixtures, the conventional true value is within the 95% confidence interval of the experimentally determined abundances. The trueness was calculated as the difference between the average fractional abundance and the corresponding conventional true value: the obtained values scatter around the respective conventional true value (-0.39% to $+2.62\%$).

To evaluate quantification of a low abundant glycoform, we determined the trueness of A2G0F/A2G1F variant fractional abundance (Figure 5(b)). In this case, the average fractional abundances were all below the corresponding conventional true values with deviations ranging from -0.34% to -2.38% . In order to assess repeatabilities, relative standard deviations (RSDs) for fractional abundances derived from five measurements were calculated (Supplementary material, spreadsheets E-13). RSDs ranged from 1.6% to 2.7% for the higher abundant A2G0F/A2G0F variant, and from 4.8% to 8.7% for the lower abundant variant A2G0F/A2G1F.

Absolute quantification of the intact mAb

Using the reference product of known concentration as the calibration standard, concentration-response curves in a range

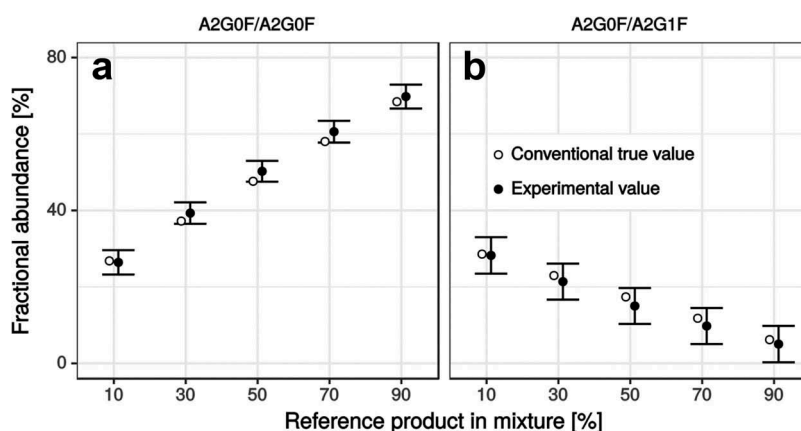


Figure 5. Trueness and precision for relative quantification of intact mAb glycoforms A2G0F/A2G0F (a) and A2G0F/A2G1F (b). Conventional true values obtained from calculation of concentration-response curves of pure day 5 (0%) and pure reference product (100%) samples. Experimental values were obtained from five technical replicates of the respective dilutions. Error bars indicate 95% confidence interval. Experimental details are provided in the Supplementary material, spreadsheets E-12 and E-13.

of 0.25–250 ng μL^{-1} were generated based on UV detection (Supplementary material, spreadsheet E-14). The lower limits of detection (LOD) and quantification (LOQ) were determined as 1.11 ng μL^{-1} and 3.34 ng μL^{-1} , respectively. Calibration functions in the range of 2.50 to 12.5 ng μL^{-1} and 25.0 to 250 ng μL^{-1} were found to be linear upon Mandel's testing with relative process standard deviations V_{x0} of 4.85% and 4.95%, respectively (Supplementary material, spreadsheet E-14). Taking into account the calibration function ranging from 2.50 to 12.5 ng μL^{-1} , absolute quantification of the intact mAb in fermentation samples and capture eluate yielded concentrations of 67.2 ng μL^{-1} (day 5), 434.3 ng μL^{-1} (day 10), 1575.7 ng μL^{-1} (day 14) and 2578.8 ng μL^{-1} (capture eluate). The amount of target protein therefore increased more than 23-fold between day 5 and day 14 of fermentation. RSDs of the determined concentrations were below 4.5%, demonstrating the reliability of UV-based quantification. Robustness was assessed according to the International Council for Harmonisation of Technical Requirements for Pharmaceuticals for Human Use (ICH) guidelines Q2(R1) considering six replicates at the lower, the middle and the upper range of the concentration response curve, respectively. Intra- and interday robustness of the chromatographic method is demonstrated by RSDs below 0.27% with regard to retention time (Table S-4). RSDs of other critical peak parameters, including peak area, peak height, and peak width at half height, were below 4.85%, with the exception of the lowest concentration (2.5 ng μL^{-1}).

Discussion

The emergence of sensitive high resolution mass spectrometers allows in-depth characterization of intact mAbs with unprecedented information density.³⁴ Moreover, hyphenation to HPLC facilitates upfront separation of mAb variants and truncation products and enables online analysis.³⁹ These advantages may be exploited for the analysis of multiple quality attributes in the course of biopharmaceutical fermentation processes. However, as conventionally employed bottom-up HPLC-MS workflows involve elaborate sample preparation, real-time online monitoring of an ongoing fermentation process is not readily feasible. The workflow described here for multiple attribute monitoring of a therapeutic mAb in the course of fermentation requires minimal sample preparation that can be completed within five minutes, followed by HPLC-UV-MS analysis. Based on the acquired mass spectra and known sequence of the target protein, mAb variants and truncation products can be identified.

More specifically, the direct analysis of mAb samples applied here allows detection of truncation products, which would be difficult to identify upon proteolytic digestion in a bottom-up approach. Although control mechanisms in mammalian cells ensure secretion of fully assembled mAb molecules only,⁴² certain mAb variants, *e.g.*, HC₂ and LC₂, have been described to evade control by specific folding of the variable domain.^{34,43–46} In addition, elevated levels of free LC have been proposed as indicators for increased productivity and cell viability of host cells for mAb production.^{47,48} The respective mAb variants identified in this study may therefore indeed result from aberrant secretion during fermentation or

from degradation of the intact mAb in the course of fermentation. Degradation of intact mAb during ESI is unlikely, as truncated variants were separated from intact mAb by HPLC before ionization (Figure 1). Individual mAb variants were relatively quantified at >1% by UV-spectroscopy as well as by MS, conforming with pharmaceutical impurity profiling that typically involves determination of fractional abundances.⁴⁹ However, different response factors in UV-spectroscopy and MS have to be considered, especially for low abundant species.

The mass accuracy determined for the applied HPLC-MS workflow suggests that mAb variants differing in molecular mass by more than 3 Da, *i.e.*, ~20 ppm for an intact mAb, may readily be discerned by MS. This, however, is only true for a mass spectrum of a pure compound. As closely related protein species are often insufficiently separated by HPLC, the acquired mass spectra may contain co-eluting variants. Yet, distinction of co-eluting variants by MS is limited by the width of the natural isotopic pattern (Figure S-10A). Based on a simulation of the isotopic envelope for a 10:1 mixture of two intact mAb variants, a lower limit in resolution of two mAb species differing by 80 Da can be estimated (Figure S-10A, C). Intact mAb variants with an absolute mass difference of more than 80 Da would thus be distinguishable at a relative concentration of 10%. Considering characteristic mass shifts of common PTMs, the following modifications are expected to be resolvable for an intact mAb under the above described conditions (mass differences in parentheses): sialylation (+291 Da), glycation (+162 Da), terminal lysine variants (+128 Da), phosphorylation (+80 Da). On the other hand, small mass shifts as induced by succinimide formation (–18 Da), pyroglutamate formation (–18 Da), or oxidation (+16 Da) will not be resolvable at the intact mAb level.⁵⁰ Under the described conditions, mass shifts down to ± 32 Da may be resolved on the HC, while delta masses down to ± 18 Da may be discerned on the LC level (Figure S-10A, D). With regard to sequence variants, only amino acid exchanges leading to mass shifts of more than ± 80 Da can be discerned at the intact mAb level, as indicated in Figure S-10B (green area). Interestingly, C-terminal lysine variants were neither detected in the reference product nor in fermentations samples, implying exhaustive processing of these two amino acids.

Glycosylation patterns of therapeutic proteins may be obtained by direct infusion of highly purified protein into the mass spectrometer.^{34,51} This approach, however, is not feasible for fermentation broth containing a multitude of compounds. Yet, mAb variants and truncation products may be efficiently separated online from other compounds present in the sample (Figure 1, Figure S-5), rendering preceding affinity purification dispensable. Mass spectra of the intact mAb revealed different glycosylation patterns for various fermentation samples. Annotation of specific glycoforms based on a CHO cell *N*-glycan library provided insights into actual pairing of *N*-glycan structures in dimeric mAb, whereas information obtained at the glycopeptide level is restricted to the pool of observed glycan structures. Remarkably, our approach also readily facilitates a relative quantification of glycoforms lacking core fucose, which may be an important molecular attribute relevant for the ADCC potency of the antibody. Limitations of this approach arise from the presence of two *N*-glycosylation sites

and the existence of isobaric *N*-glycan structures. For in-depth structural characterization revealing monosaccharide stereoisomers, linkages, anomeric configurations, and glycan branching, in-depth analysis of released *N*-glycans and glycopeptide analysis are thus still indispensable. Moreover, determination of *N*-glycolylneuraminic acid and α 1-3-linked galactose, which usually occur at low levels, are not amenable to our workflow and require orthogonal analytical methods.

While peptide mapping allowed determination of glycation sites, relative quantification of glycated mAb species was achievable at the level of the intact protein. The determined glycation levels were then considered for relative quantification of mAb *N*-glycoforms at the intact protein level as the additional hexose residues bias the quantification.³⁴ Indeed, correction for glycation significantly affected relative quantification of *N*-glycoforms as exemplified by a change from 61.6% to 76.7% fractional abundance of the A2G0F/A2G0F variant in the reference product (Supplementary material, spreadsheet E-11). On the other hand, the fractional abundance of the galactosylated mAb variant A2G1F/A2G1F was corrected from 3.5% to 0.70%. The level of terminal galactosylation of mAb *N*-glycans is of importance, as it may affect CDC activity by increased binding to the complement component C1q.^{52–54} The effect of terminal galactose residues on ADCC is still controversial: while most studies report no effect,^{52–54} others describe a slight increase in ADCC.^{55,56} In contrast, afucosylated *N*-glycoforms such as the detected A2G0/A2G0F variant are considered major drivers for ADCC activity.^{17,18,53,55,57} The ability to identify and relatively quantify these glycoforms at the intact protein level is therefore highly relevant for monitoring of mAb production processes. In fact, the A2G0/A2G0F variant could be identified and relatively quantified in a sample from fermentation broth displaying an absolute mAb concentration below 10 ng μ L⁻¹ (e.g., day 10 diluted to 8.7 ng μ L⁻¹).

In addition to the in-process monitoring of multiple quality attributes, UV-spectroscopy implemented in the described workflow enabled absolute quantification of the intact mAb in fermentation broth samples. RSDs of critical peak parameters determined in accordance with ICH guidelines Q2 R1 were comparable to previous studies describing absolute quantification of intact proteins by UV-spectroscopy.^{40,58,59}

In summary, we describe a fast and powerful HPLC-MS-based workflow for monitoring of multiple attributes of mAbs directly in fermentation broth, including intact molecular mass, *N*-glycosylation patterns, glycation, protein truncation, as well as C- and N-terminal modifications. The evaluated robustness and precision for quantification of mAb variants renders our dilute-and-shoot approach highly attractive for industrial applications. Besides clone selection and process optimization during early drug development, the workflow may be applied for batch-to-batch analysis of originator molecules or comparability studies of biosimilars and their reference drug product.

Materials & methods

Materials

Acetonitrile (ACN, \geq 99.9%, Cat.Nr. 1.00030.2500) and methanol (MeOH, \geq 99.9%, Cat.Nr. 83638.320) were obtained from

VWR International. Ammonium hexafluorophosphate (AHFP, 99.98%, Cat.Nr. 216593), tris(2-carboxyethyl) phosphine hydrochloride (TCEP, \geq 98.0%, Cat.Nr. 75259-1G), trifluoroacetic acid (TFA, \geq 99.0%, Cat.Nr. 74564-10ML-F) and ribonuclease A from bovine pancreas (RibA, Cat.Nr. R5503-100MG) were purchased from Sigma-Aldrich (Vienna, Austria). Ammonium acetate (\geq 98.0%, Cat.Nr. 101116) was purchased from Merck. Ultrapure water used for all experiments was produced in-house by a Millipore Integral 3 from Merck/Millipore (Billerica, MA, USA). Peptide-*N*-glycosidase F (PNGase F, Cat.Nr. P0704S) was obtained from New England BioLabs. SMART Digest™ Trypsin Kit was kindly provided from Thermo Fisher Scientific (Germering, Germany).

Sample preparation

For the measurement of the concentration-response curves, the reference drug product was diluted to the respective concentrations in 25% ACN + 0.050% TFA. Additionally, ribonuclease A (RibA) was added at a concentration of 100 ng μ L⁻¹ as carrier protein for diminishing loss of the calibrant because of adsorption to glass surfaces, especially of the low concentrated solutions, as previously described.⁴⁰

The samples from fermentation broth (day 5, day 10, day 14) and the capture eluate (day 15 after protein A purification) were centrifuged for three minutes at 14,000 g at 4°C. The required volume of the supernatant was diluted in 25% ACN + 0.050% TFA and 100 ng μ L⁻¹ RibA. As the protein concentrations of fermentation samples and capture eluate were unknown, a trial injection of a 1:10 (*v/v*) dilution of each sample was performed before preparing the final dilutions. If a 1:10 diluted sample exceeded a value of 800 mAU measured with the UV detector, the samples were further diluted to avoid overloading of the column. Samples were finally diluted as follows: day 5 (1:10), day 10 (1:50), day 14 (1:200), capture eluate (1:400).

For determination of the glycation level, 500 ng mAb of each sample were diluted in 20 μ L of 175 mmolL⁻¹ ammonium acetate, supplemented with 0.50 μ L (250 units) of PNGase F and incubated for three hours at 37°C. Samples were then diluted 1:4 with 25% ACN + 0.050% TFA.

For peptide mapping, 100 ng of each sample were diluted to a concentration of 2.0 ng μ L⁻¹ in 50 μ L ultrapure water. After addition of 150 μ L of SMART Digest™ buffer the samples were incubated at 70°C and 900 rpm for one hour. Disulfides were reduced by addition of 5 mM TCEP and incubation at 70°C and 900 rpm for 15 min.

High-performance liquid chromatography

Chromatographic separation of mAb variants was performed on a Thermo Scientific™ UltiMate™ 3000 Rapid Separation Binary system (Thermo Fisher Scientific, Germering, Germany) at a flow rate of 200 μ L min⁻¹ employing a monolithic PS-DVB Thermo Scientific™ ProSwift™ RP-10R column (50 \times 1.0 mm i.d., Thermo Fisher Scientific, Sunnyvale, CA, USA), operated at a temperature of 70°C. Mobile phase A was composed of H₂O + 0.050% TFA, mobile phase B of ACN + 0.050% TFA. The total run time for one sample was fifteen minutes. The separation started at 25% B for 2 min followed

by a linear gradient of 25–50% B in 5.0 min, after this eluent B was increased to 80% for 3.0 min, followed by re-equilibration at 25% B for 5.0 min. Injection was carried out in in-line split-loop mode, injection volume was kept at ten microliters for each sample. UV-detection was carried out at 214 nm with a 2.5 μL flow cell.

For acquisition of peptide mapping data, 250 ng of digested sample were loaded onto the same HPLC system utilizing a Thermo Scientific™ Hypersil GOLD™ aQ C18 column (100 \times 1.0 mm i.d., 1.9 μm particle size, 175 Å pore size, Thermo Fisher Scientific, Sunnyvale, CA, USA) at a flow rate of 60 $\mu\text{L}\cdot\text{min}^{-1}$ operated at a temperature of 50°C. The gradient applied was: 2.0% B for 5.0 min, 5.0–10.0% B in 5.0 min, 10.0–40.0% B in 60 min, 100% B for 5.0 min, and 2.0% B for 25 min.

Mass spectrometry

Mass spectrometry was conducted on a benchtop quadrupole-Orbitrap instrument (Thermo Scientific™ Q Exactive™) equipped with a Thermo Scientific™ Ion Max™ source with a heated electrospray ionization (HESI) probe, both from Thermo Fisher Scientific (Bremen, Germany). Additionally, an MXT715-000 – MX Series II Switching Valve from IDEX Health & Science LLC (Oak Harbor, WA, USA) was installed between HPLC system and the HESI probe in order to divert low molecular compounds eluting in the hold-up volume to waste during the first minute of elution. Mass calibration of the instrument was carried out with Thermo Scientific™ Pierce™ LTQ Velos ESI Positive Ion Calibration Solution (Cat.Nr. 88323) from Thermo Fisher Scientific, high-mass calibration with ammonium hexafluorophosphate.

The instrument was tuned by direct infusion of 1 $\text{mg}\cdot\text{mL}^{-1}$ of the reference mAb drug product in 35% ACN + 0.050% TFA at a flowrate of 1 $\mu\text{L}\cdot\text{min}^{-1}$ into a T-piece connected with the HPLC pumping 35% ACN + 0.050% TFA at a flow rate of 200 $\mu\text{L}\cdot\text{min}^{-1}$. The optimized instrument settings were as follows: source heater temperature of 250°C, spray voltage of 4.0 kV, sheath gas flow of 15 arbitrary units, auxiliary gas flow of 5.0 arbitrary units, capillary temperature of 275°C, source-induced dissociation of 80.0 eV, S-lens radio frequency (RF) level of 80.0, automatic gain control (AGC) target of 3e6 and a maximum injection time of 150 ms. Measurements were performed in full scan mode in a range of m/z 1,800–5,500 at a resolution of 17,500 at m/z 200 and averaging of 10 microscans.

For peptide mapping, the source heater temperature was set to 100°C, spray voltage to 3.5 kV, sheath gas flow to 10 arbitrary units, auxiliary gas flow of 5.0 arbitrary units, capillary temperature to 300°C and S-lens RF level to 60.0. Each scan cycle consisted of a full scan at a scan range of m/z 350–2,000 with an AGC target of 1e6 (maximum injection time of 150 ms, resolution setting of 70,000), followed by 5 data-dependent higher-energy collisional dissociation scans at 28% normalized collision energy with an isolation window of 2 m/z and an AGC target of 1e5 (maximum injection time of 150 ms, resolution setting of 17,500). Dynamic exclusion was set to 10 seconds.

Data evaluation

Data acquisition of intact mAb separation and peptide mapping was conducted using Thermo Scientific™ Dionex™ Chromeleon™ 7.2 chromatography data system software (Thermo Fisher Scientific, Germering, Germany). Deconvolution and peak assignment of mass spectra was performed with Thermo Scientific™ BioPharma Finder™ 3.0 software and an integrated CHO cell glycan database (Thermo Fisher Scientific, San Jose, CA, USA). For intact mAb, the integrated ReSpect algorithm was used; for peptide mapping, the Xtract algorithm was utilized. Specific details for the deconvolution of individual spectra are provided in the Supplementary material. XICCs for mAb glycation and glycosylation variants were calculated based on the FWHM of the respective experimentally observed most intense charge state at the resolution settings used for mass spectrometry simulated in Thermo Scientific™ Xcalibur™ 3.0.63 software (Figure S-7). For calculation of XICCs, linearity testing and data assembly a spreadsheet (Microsoft Excel 2010, vers. 14.0.7192.5000, 32-bit, Microsoft Corporation, Redmond, WA, USA) was generated which is also available as Supplementary material.

For correction of relative *N*-glycoform quantification, we implemented an algorithm that identifies all sets of glycoforms whose monosaccharide compositions become identical upon glycation. The algorithm then employs a graph theoretical approach, a mathematical model for pairwise relations, to correct for glycation-induced transfers of abundance between these overlapping sets of glycoforms. For instance, part of the abundance observed for A2G1F/A2G1F actually results from singly-glycated A2G0F/A2G1F and doubly-glycated A2G0F/A2G0F, since each of these proteoforms comprises eight hexoses, eight *N*-acetylhexosamines and two fucoses. Moreover, A2G1F/A2G1F loses part of its actual abundance to A2G1F/A2G2F and A2G2F/A2G2F if glycated once or twice, respectively. Consequently, the algorithm will eliminate these glycation-associated changes in A2G1F/A2G1F abundance. Details on the correction algorithm will be described elsewhere. The mass spectrometry data have been deposited to the ProteomeXchange Consortium via the PRIDE⁶⁰ partner repository with the dataset identifier PXD011017.

Acknowledgments

The financial support by the Austrian Federal Ministry for Digital and Economic Affairs, the National Foundation of Research, Technology, and Development, and by a Start-up Grant of the State of Salzburg is gratefully acknowledged. We also acknowledge financial support by the Open Access Publication Fund of the University of Salzburg.

Disclosure of potential conflicts of interest

The authors declare the following competing financial interest(s): Johann Holzmann is employee of Novartis, Martin Samonig is employed at Thermo Fisher Scientific GmbH. Both companies provide financial support for the Christian Doppler Laboratory for Innovative Tools for Biosimilar Characterization. The salaries of Therese Wohlschlager and Wolfgang Esser-Skala are fully funded - Christian G. Huber's salary is partly funded by the Christian Doppler Laboratory for Biosimilar Characterization. The authors declare no other competing financial interest.

Funding

This work was supported by the Christian Doppler Forschungsgesellschaft [Christian Doppler Laboratory for Biosimilar Characterization]

Abbreviations

ACN	acetonitrile
ADCC	antibody-dependent cell-mediated cytotoxicity
AGC	automatic gain control
AHFP	ammonium hexafluorophosphate
AMBR™	advanced microscale bioreactor
CDC	complement-dependent cytotoxicity
CDR	complementarity determining region
CHO	Chinese hamster ovary
CQA	critical quality attribute
ESI	electrospray ionization
FWHM	full width at half maximum
HC	heavy chain
HC ₂	heavy chain dimer
HPLC	high-performance liquid chromatography
ICH	International Council for Harmonisation of Technical Requirements for Pharmaceuticals for Human Use
IP-RP	ion-pair reversed-phase
LC	light chain
LC ₂	light chain dimer
LOD	limit of detection
LOQ	limit of quantification
mAb	monoclonal antibody
MAM	multiple attribute monitoring
MeOH	methanol
MS	mass spectrometry
PAT	process analytical technology
PNGase F	peptide-N-glycosidase F
PS-DVB	poly(styrene-divinylbenzene)
RF	radio frequency
RibA	ribonuclease A
RSD	relative standard deviation
TCEP	tris(2-carboxyethyl) phosphine hydrochloride
TFA	trifluoroacetic acid
TICC	total ion current chromatogram
UV	ultraviolet
XICC	extracted ion current chromatogram

ORCID

Christof Regl  <http://orcid.org/0000-0002-7938-4494>
 Therese Wohlschlager  <http://orcid.org/0000-0001-9359-6744>
 Wolfgang Esser-Skala  <http://orcid.org/0000-0002-7350-4045>
 Iris Wagner  <http://orcid.org/0000-0001-9198-4532>
 Johann Holzmann  <http://orcid.org/0000-0003-2622-4072>
 Christian G. Huber  <http://orcid.org/0000-0001-8358-1880>

References

- Li F, Vijayasankaran N, Shen AY, Kiss R, Amanullah A. Cell culture processes for monoclonal antibody production. *MAbs*. 2010;2:466–79.
- Wurm FM. Production of recombinant protein therapeutics in cultivated mammalian cells. *Nat Biotechnol*. 2004;22:1393–98. doi:10.1038/nbt1026.
- Zhang J, Zhou H, Ji Z, Regnier F. Monoclonal antibody production with on-line harvesting and process monitoring. *J Chromatogr B Biomed Sci Appl*. 1998;707:257–65.
- Miller AK, Hambly DM, Kerwin BA, Treuheit MJ, Gadgil HS. Characterization of site-specific glycation during process development of a human therapeutic monoclonal antibody. *J Pharm Sci*. 2011;100:2543–50. doi:10.1002/jps.22504.
- Fischer S, Hoernschemeyer J, Mahler HC. Glycation during storage and administration of monoclonal antibody formulations. *Eur J Pharm Biopharm*. 2008;70:42–50. doi:10.1016/j.ejpb.2008.04.021.
- Vogt W. Oxidation of methionyl residues in proteins: tools, targets, and reversal. *Free Radic Biol Med*. 1995;18:93–105.
- Houde D, Kauppinen P, Mhatre R, Lyubarskaya Y. Determination of protein oxidation by mass spectrometry and method transfer to quality control. *J Chromatogr A*. 2006;1123:189–98. doi:10.1016/j.chroma.2006.04.046.
- Beck A, Wagner-Roussel E, Ayoub D, Van Dorsseleer A, Sanglier-Cianferani S. Characterization of therapeutic antibodies and related products. *Anal Chem*. 2013;85:715–36. doi:10.1021/ac3032355.
- Rosati S, van Den Bremer ET, Schuurman J, Parren PW, Kamerling JP, Heck AJ. In-depth qualitative and quantitative analysis of composite glycosylation profiles and other micro-heterogeneity on intact monoclonal antibodies by high-resolution native mass spectrometry using a modified Orbitrap. *MAbs*. 2013;5:917–24. doi:10.4161/mabs.26282.
- Liu H, Gaza-Bulseco G, Lundell E. Assessment of antibody fragmentation by reversed-phase liquid chromatography and mass spectrometry. *J Chromatogr B Analyt Technol Biomed Life Sci*. 2008;876:13–23. doi:10.1016/j.jchromb.2008.10.015.
- Glassy MC, Tharakan JP, Chau PC. Serum-free media in hybridoma culture and monoclonal antibody production. *Biotechnol Bioeng*. 1988;32:1015–28. doi:10.1002/bit.260320809.
- Cordoba AJ, Shyong B-J, Breen D, Harris RJ. Non-enzymatic hinge region fragmentation of antibodies in solution. *J Chromatogr B*. 2005;818:115–21. doi:10.1016/j.jchromb.2004.12.033.
- Schmid G, Blanch HW, Wilke CR. Hybridoma growth, metabolism, and product formation in HEPES-buffered medium: I. Effect of passage number. *Biotechnol Lett*. 1990;12:627–32. doi:10.1007/BF01088184.
- Reusch D, Tejada ML. Fc glycans of therapeutic antibodies as critical quality attributes. *Glycobiology*. 2015;25:1325–34. doi:10.1093/glycob/cwv065.
- Meier S, Duus J. Carbohydrate dynamics: antibody glycans wiggle and jiggle. *Nat Chem Biol*. 2011;7:131–32. doi:10.1038/nchembio.526.
- Reichert JM, Valge-Archer VE. Development trends for monoclonal antibody cancer therapeutics. *Nat Rev Drug Discovery*. 2007;6:349–56. doi:10.1038/nrd2241.
- Shields RL, Lai J, Keck R, O'Connell LY, Hong K, Meng YG, Weikert SHA, Presta LG. Lack of fucose on human IgG1 N-linked oligosaccharide improves binding to human FcγRIII and antibody-dependent cellular toxicity. *J Biol Chem*. 2002;277:26733–40. doi:10.1074/jbc.M202069200.
- Pereira NA, Chan KF, Lin PC, Song Z. The “less-is-more” in therapeutic antibodies: afucosylated anti-cancer antibodies with enhanced antibody-dependent cellular cytotoxicity. *MAbs*. 2018;10:693–711. doi:10.1080/19420862.2018.1466767.
- Quan C, Alcalá E, Petkovska I, Matthews D, Canova-Davis E, Taticek R, Ma S. A study in glycation of a therapeutic recombinant humanized monoclonal antibody: where it is, how it got there, and how it affects charge-based behavior. *Anal Biochem*. 2008;373:179–91. doi:10.1016/j.ab.2007.09.027.
- Kennedy DM, Skillen AW, Self CH. Glycation of monoclonal antibodies impairs their ability to bind antigen. *Clin Exp Immunol*. 1994;98:245–51.
- Hmiel LK, Brorson KA, Boyne MT 2nd. Post-translational structural modifications of immunoglobulin G and their effect on biological activity. *Anal Bioanal Chem*. 2015;407:79–94. doi:10.1007/s00216-014-8108-x.
- Mo J, Jin R, Yan Q, Sokolowska I, Lewis MJ, Hu P. Quantitative analysis of glycation and its impact on antigen binding. *MAbs*. 2018;10:406–415. doi:10.1080/19420862.2018.1438796.
- Reusch D, Habegger M, Selman MH, Bulau P, Deelder AM, Wuhrer M, Engler N. High-throughput work flow for IgG Fc-glycosylation analysis of biotechnological samples. *Anal Biochem*. 2013;432:82–89. doi:10.1016/j.ab.2012.09.032.

24. Pabst M, Altmann F. Glycan analysis by modern instrumental methods. *Proteomics*. 2011;11:631–43. doi:10.1002/pmic.201000517.
25. Huhn C, Selman MH, Ruhaak LR, Deelder AM, Wuhrer M. IgG glycosylation analysis. *Proteomics*. 2009;9:882–913. doi:10.1002/pmic.200800715.
26. Rogers RS, Nightlinger NS, Livingston B, Campbell P, Bailey R, Balland A. Development of a quantitative mass spectrometry multi-attribute method for characterization, quality control testing and disposition of biologics. *MAbs*. 2015;7:881–90. doi:10.1080/19420862.2015.1069454.
27. Xu W, Jimenez RB, Mowery R, Luo H, Cao M, Agarwal N, Ramos I, Wang X, Wang J. A Quadrupole Dalton-based multi-attribute method for product characterization, process development, and quality control of therapeutic proteins. *MAbs*. 2017;9:1186–96. doi:10.1080/19420862.2017.1364326.
28. Bondarenko PV, Second TP, Zabrouskov V, Makarov AA, Zhang Z. Mass measurement and top-down HPLC/MS analysis of intact monoclonal antibodies on a hybrid linear quadrupole ion trap-Orbitrap mass spectrometer. *J Am Soc Mass Spectrom*. 2009;20:1415–24. doi:10.1016/j.jasms.2009.03.020.
29. Wang T, Hoi KM, Stockmann H, Wan C, Sim LC, Shi Jie Tay N, Poo CH, Woen S, Yang Y, Zhang P, et al. LC/MS-based intact IgG and released Glycan analysis for bioprocessing applications. *Biotechnol J*. 2018;13:e1700185. doi:10.1002/biot.v13.4.
30. Zhang Z, Pan H, Chen X. Mass spectrometry for structural characterization of therapeutic antibodies. *Mass Spectrom Rev*. 2009;28:147–76. doi:10.1002/mas.20190.
31. Beck A, Sanglier-Cianferani S, Van Dorsselaer A. Biosimilar, biobetter, and next generation antibody characterization by mass spectrometry. *Anal Chem*. 2012;84:4637–46. doi:10.1021/ac3002885.
32. Dillon TM, Bondarenko PV, Rehder DS, Pipes GD, Kleemann GR, Ricci MS. Optimization of a reversed-phase high-performance liquid chromatography/mass spectrometry method for characterizing recombinant antibody heterogeneity and stability. *J Chromatogr A*. 2006;1120:112–20. doi:10.1016/j.chroma.2006.01.016.
33. Yang Y, Franc V, Heck AJR. Glycoproteomics: a balance between high-throughput and in-depth analysis. *Trends Biotechnol*. 2017;35:598–609. doi:10.1016/j.tibtech.2017.04.010.
34. Yang Y, Wang G, Song T, Lebrilla CB, Heck AJR. Resolving the micro-heterogeneity and structural integrity of monoclonal antibodies by hybrid mass spectrometric approaches. *MAbs*. 2017;9:638–45. doi:10.1080/19420862.2017.1290033.
35. Gadgil HS, Pipes GD, Dillon TM, Treuheit MJ, Bondarenko PV. Improving mass accuracy of high performance liquid chromatography/electrospray ionization time-of-flight mass spectrometry of intact antibodies. *J Am Soc Mass Spectrom*. 2006;17:867–72. doi:10.1016/j.jasms.2006.02.023.
36. Bongers J, Cummings JJ, Ebert MB, Federici MM, Gledhill L, Gulati D, Hilliard GM, Jones BH, Lee KR, Mozdzanowski J, et al. Validation of a peptide mapping method for a therapeutic monoclonal antibody: what could we possibly learn about a method we have run 100 times? *J Pharm Biomed Anal*. 2000;21:1099–128.
37. Chelius D, Rehder DS, Bondarenko PV. Identification and characterization of deamidation sites in the conserved regions of human immunoglobulin gamma antibodies. *Anal Chem*. 2005;77:6004–11. doi:10.1021/ac050672d.
38. Battersby JE, Snedecor B, Chen C, Champion KM, Riddle L, Vanderlaan M. Affinity-reversed-phase liquid chromatography assay to quantitate recombinant antibodies and antibody fragments in fermentation broth. *J Chromatogr A*. 2001;927:61–76.
39. Kuribayashi R, Hashii N, Harazono A, Kawasaki N. Rapid evaluation for heterogeneities in monoclonal antibodies by liquid chromatography/mass spectrometry with a column-switching system. *J Pharm Biomed Anal*. 2012;67–68:1–9. doi:10.1016/j.jpba.2012.04.005.
40. Forstenlehner IC, Holzmann J, Toll H, Huber CG. Site-specific characterization and absolute quantification of pegfilgrastim oxidation by top-down high-performance liquid chromatography-mass spectrometry. *Anal Chem*. 2015;87:9336–43. doi:10.1021/acs.analchem.5b02029.
41. Mohr J, Swart R, Samonig M, Böhm G, Huber CG. High-efficiency nano- and micro-HPLC - High-Resolution Orbitrap-MS platform for top-down proteomics. *Proteomics*. 2010;10:3598–609. doi:10.1002/pmic.201000341.
42. Bole DG, Hendershot LM, Kearney JF. Posttranslational association of immunoglobulin heavy chain binding protein with nascent heavy chains in nonsecreting and secreting hybridomas. *J Cell Biol*. 1986;102:1558–66.
43. Stoye CL, Stephens PE, Humphreys DP, Heywood S, Cain K, Bulleid NJ. IgG light chain-independent secretion of heavy chain dimers: consequence for therapeutic antibody production and design. *Biochem J*. 2017;474:3179–88. doi:10.1042/BCJ20170342.
44. O'Callaghan PM, McLeod J, Pybus LP, Lovelady CS, Wilkinson SJ, Racher AJ, Porter A, James DC. Cell line-specific control of recombinant monoclonal antibody production by CHO cells. *Biotechnol Bioeng*. 2010;106:938–51. doi:10.1002/bit.22769.
45. Stevens FJ, Schiffer M. Structure and properties of human immunoglobulin light-chain dimers. *Methods Mol Biol*. 1995;51:51–81. doi:10.1385/0-89603-275-2:51.
46. Lu C, Liu D, Liu H, Motchnik P. Characterization of monoclonal antibody size variants containing extra light chains. *MAbs*. 2013;5:102–13. doi:10.4161/mabs.22965.
47. Bhoskar P, Belongia B, Smith R, Yoon S, Carter T, Xu J. Free light chain content in culture media reflects recombinant monoclonal antibody productivity and quality. *Biotechnol Prog*. 2013;29:1131–39. doi:10.1002/btpr.1767.
48. Leitzgen K, Knittler MR, Haas IG. Assembly of immunoglobulin light chains as a prerequisite for secretion. A model for oligomerization-dependent subunit folding. *J Biol Chem*. 1997;272:3117–23.
49. Neu V, Bielow C, Gostomski I, Wintringer R, Braun R, Reinert K, Schneider P, Stuppner H, Huber CG. Rapid and comprehensive impurity profiling of synthetic thyroxine by ultrahigh-performance liquid chromatography-high-resolution mass spectrometry. *Anal Chem*. 2013;85:3309–17. doi:10.1021/ac303722j.
50. Regl C, Wohlschlager T, Holzmann J, Huber CG. A generic HPLC method for absolute quantification of oxidation in monoclonal antibodies and Fc-Fusion proteins using UV and MS detection. *Anal Chem*. 2017;89:8391–98. doi:10.1021/acs.analchem.7b01755.
51. Wohlschlager T, Scheffler K, Forstenlehner IC, Skala W, Senn S, Damac E, Holzmann J, Huber CG. Native mass spectrometry combined with enzymatic dissection unravels glycoform heterogeneity of biopharmaceuticals. *Nat Commun*. 2018;9:1713. doi:10.1038/s41467-018-04061-7.
52. Hodoniczky J, Zheng YZ, James DC. Control of recombinant monoclonal antibody effector functions by Fc N-glycan remodeling in vitro. *Biotechnol Prog*. 2005;21:1644–52. doi:10.1021/bp050228w.
53. Raju TS. Terminal sugars of Fc glycans influence antibody effector functions of IgGs. *Curr Opin Immunol*. 2008;20:471–78. doi:10.1016/j.coi.2008.06.007.
54. Boyd PN, Lines AC, Patel AK. The effect of the removal of sialic acid, galactose and total carbohydrate on the functional activity of Campath-1H. *Mol Immunol*. 1995;32:1311–18.
55. Thomann M, Reckermann K, Reusch D, Prasser J, Tejada ML. Fc-galactosylation modulates antibody-dependent cellular cytotoxicity of therapeutic antibodies. *Mol Immunol*. 2016;73:69–75. doi:10.1016/j.molimm.2016.03.002.
56. Houde D, Peng Y, Berkowitz SA, Engen JR. Post-translational modifications differentially affect IgG1 conformation and receptor binding. *Mol Cell Proteomics*. 2010;9:1716–28. doi:10.1074/mcp.M900540-MCP200.

57. Umana P, Jean-Mairet J, Moudry R, Amstutz H, Bailey JE. Engineered glycoforms of an antineuroblastoma IgG1 with optimized antibody-dependent cellular cytotoxic activity. *Nat Biotechnol.* 1999;17:176–80. doi:10.1038/6179.
58. Yin Y, Han G, Zhou J, Dillon M, McCarty L, Gavino L, Ellerman D, Spiess C, Sandoval W, Carter PJ. Precise quantification of mixtures of bispecific IgG produced in single host cells by liquid chromatography-Orbitrap high-resolution mass spectrometry. *MAbs.* 2016;8:1467–76. doi:10.1080/19420862.2016.1232217.
59. Navas N, Herrera A, Martinez-Ortega A, Salmeron-Garcia A, Cabeza J, Cuadros-Rodriguez L. Quantification of an intact monoclonal antibody, rituximab, by (RP)HPLC/DAD in compliance with ICH guidelines. *Anal Bioanal Chem.* 2013;405:9351–63. doi:10.1007/s00216-013-7368-1.
60. Vizcaino JA, Csordas A, Del-Toro N, Dianas JA, Griss J, Lavidas I, Mayer G, Perez-Riverol Y, Reisinger F, Ternent T, et al. 2016 update of the PRIDE database and its related tools. *Nucleic Acids Res.* 2016;44:11033. doi:10.1093/nar/gkw880.